# Check for updates

### MATERIALS SCIENCE

# A low-temperature, one-step synthesis for monazite can transform monazite into a readily usable advanced nuclear waste form

Yunping Zhoujin<sup>1,2</sup>, Hunter B. Tisdale<sup>1,2</sup>, Navindra Keerthisinghe<sup>2</sup>, Gregory Morrison<sup>1,2</sup>, Mark D. Smith<sup>2</sup>, Joke Hadermann<sup>3</sup>, Theodore M. Besmann<sup>1</sup>, Jake Amoroso<sup>4</sup>, Hans-Conrad zur Loye<sup>1,2,4</sup>\*

It has been demonstrated that monazite-type materials are excellent candidates for nuclear waste forms, and hence, their facile synthesis is of great importance for the needed sequestration of existing nuclear waste. The synthesis of monazite, LaPO<sub>4</sub>, requires inconveniently high temperatures near 1000°C and generally involves the conversion of the presynthesized rhabdophane, LaPO<sub>4</sub>•nH<sub>2</sub>O, to the LaPO<sub>4</sub> monazite phase. During this structure transformation, the rhabdophane converts irreversibly to the thermodynamically stable monoclinic monazite structure. A low-temperature (185° to 260°C) mild hydrothermal acid-promoted synthesis of monazite is described that can both transform presynthesized rhabdophane or assemble reagents to the monoclinic monazite structure. The pH dependence of this reaction is detailed, and its applicability to the  $LnPO_4$  (Ln = La, Ce, Pr, Nd, Sm-Gd),  $Ca_{0.5}Th_{0.5}PO_4$ , and  $Sr_{0.5}Th_{0.5}PO_4$  systems is discussed. The crystal growth of  $Ca_{0.5}Th_{0.5}PO_4$  and  $Sr_{0.5}Th_{0.5}PO_4$  is described, and their crystal structures were reported. In situ x-ray diffraction studies, performed as a function of temperature, provide insight into the structure transformation process.

Copyright © 2025 The Authors, some rights reserved; exclusive licensee American Association for the Advancement of Science. No claim to original U.S. Government Works. Distributed under a Creative Commons Attribution NonCommercial License 4.0 (CC BY-NC).

### INTRODUCTION

Novel nuclear waste forms can have a transformative effect in reducing the environmental and financial costs of sequestering certain types of nuclear waste (1, 2). A waste form's performance is of critical importance as it is the barrier between the radiological (or chemical) hazard and the environment. Discovering and tailoring waste forms that can perform as good as or better than high-level waste (HLW) glasses but that require less energy to produce or that incorporate greater concentrations of radionuclides have the potential to reduce the long-term financial and environmental cost of processing and immobilizing nuclear wastes.

The vast majority of the 380,000 m³ of the nation's HLW has been stored in tanks at the Savannah River Site (SRS) in South Carolina and the Hanford Site in Washington State for decades (3) where it is being converted (or awaiting conversion) into glass before final disposal. Although more than 4000 canisters of HLW glass have been produced at SRS since production began in the 1990s, that mission is only about half completed, and no glass has been produced at Hanford. These missions are decades long and as the anticipated time and cost of processing the US Department of Energy's legacy tank waste continue to increase, waste form alternatives that provide the requisite performance and quality but that can be produced at greater rates or reduced costs are increasingly of interest.

While alkali borosilicate glasses dominate efforts to convert HLW to a durable waste form, they do have limitations including (i) limited concentrations of certain radionuclides and (ii) requiring relatively high temperatures to process. The former leads to lower waste loadings and concomitant high costs driven by the generation of greater volumes of glass. The latter can also drive costs as

the potential for volatilization of some waste elements requires the process to preseparate or capture the evaporated radionuclides.

Actinide series elements, for example, are one area where alkali borosilicate glasses are limited in waste loading, typically 10 to 20 times lower than in ceramics (4, 5), and where new waste forms are hence desirable. This is in line with a 1996 National Academy of Sciences workshop (6), which noted that alternatives to glass waste forms could be needed for containing exceptionally long-lived radionuclides, e.g., actinides. The current work is an investigation of a lower temperature route to a crystalline monazite waste form that permits high actinide waste loading in a potentially environmentally stable form.

One reason to consider crystalline structures for nuclear waste forms, such as monazite, is their ability to contain the radioactive elements in specific crystallographic locations that can create extremely stable coordination environments and, furthermore, can allow for specific elemental substitutions to accommodate elements in different oxidation states and ionic radii (7). The use of phosphates as potential single- or multiradionuclide-containing ceramic waste forms has been previously considered and continues to be of interest (8), as the phosphates sinter well, have good environmental stability, and exhibit high radiation tolerance (9).

The considered monazite-based phosphate phases can host a variety of actinide elements, including U, Pu, and the minor actinides, such as Np, Am, and Cm (10). In nature, the mineral monazite has been found to contain up to ~15% U and ~50% Th. Despite the significant internal radiation dose from the U and Th isotopes over hundreds of millions of years, the mineral samples retained crystallinity (11), which has been the reason for interest in these structures for crystalline waste forms. The radiation resistance is believed to be due to low temperatures self-healing (12), as its observed low critical amorphization temperature of 200° to 300°C (9) promotes lattice relaxation at modest temperatures. These attributes make these monazite-type materials excellent candidates for waste forms, particularly for sequestering high concentrations of actinides.

<sup>&</sup>lt;sup>1</sup>Center for Hierarchical Waste form Materials, Columbia, SC 29208, USA. <sup>2</sup>Department of Chemistry and Biochemistry, University of South Carolina, Columbia, SC 29208, USA. <sup>3</sup>Department of Physics, University of Antwerp, 2020 Antwerpen, Belgium. <sup>4</sup>Savannah River National Laboratory, Aiken, SC 29808, USA.

<sup>\*</sup>Corresponding author. Email: zurloye@mailbox.sc.edu

An extensive literature exists (8, 12) that discusses monazite as a nuclear waste form and its adaptation for use with diverse waste streams (12). Nonetheless, there is limited information on the crystal chemistry of monazite-type materials, partly due to the difficulty of growing single crystals of the more complex compositions for precise structure determination. Growing and analyzing monazite and cheralite crystals can help us to better understand the crystal chemistry of actinide containing monazite-type materials.

A barrier to the consideration of phosphate materials as waste forms has been the high processing temperature necessary to remove water from the hydrated precursors. Assuming that the rare-earths can reasonably represent actinides, the hydrated forms adopt two distinct structural types: the hydrated rhabdophane, LnPO<sub>4</sub>•nH<sub>2</sub>O (Ln = La-Gd), and the churchite (Ln = Gd-Lu, Y) forms, which are precursors to the anhydrous monazite and xenotime structures, respectively (table S1). The direct synthesis of monazite, LnPO<sub>4</sub>, or cheralite, Ca<sub>0.5</sub>Th<sub>0.5</sub>PO<sub>4</sub>, is thus complicated by the ready formation, in aqueous synthesis, of rhabdophane or grayite, respectively, the hydrated form of monazite,  $LnPO_4 \cdot n(H_2O)$  (Ln = La-Gd), and  $Ca_{0.5}$ Th<sub>0.5</sub>PO<sub>4</sub>•n(H<sub>2</sub>O), the hydrated form of cheralite. As it is essential that water be excluded from the transuranic-containing waste form to avoid water radiolysis that results in reactive species such as H<sub>2</sub>O<sub>2</sub> and H<sub>2</sub>, it is necessary to convert the hydrated forms to the anhydrous monazite-type structures (13). This transformation can readily be achieved; however, it requires very high temperatures (Fig. 1) (14-16). For this reason, finding synthetic routes that can lead to crystalline monazite and cheralite materials under mild conditions, either directly or via the rhabdophane and grayite precursors, is important for the development of phosphate based multi-element ceramic waste forms.

The monazite structure,  $LnPO_4$  (Ln = La-Gd) (Fig. 2), is monoclinic and crystallizes in the  $P2_1/n$  space group, where the rare earth cation is in a low-symmetry  $LnO_9$  coordination environment with nine different Ln-O bond lengths. The  $LnO_9$  polyhedra share edges with each other resulting in a 3D structure that is further connected via corner and edge sharing  $PO_4$  units (Fig. 2). The 9 unique Ln-O bond distances make the monazite structure compositionally very versatile as the extremely distorted rare earth polyhedra readily

accommodate a variety of cations with oxidation states of +2, +3, and +4 and different ionic radii. The closely related xenotime structure,  $LnPO_4$  (Ln = Gd-Lu, Y), is tetragonal, space group  $I4_1/amd$ , contains  $LnO_8$  polyhedra, and crystallizes in the  $ZrSiO_4$  structure type. This modification forms for the smaller rare earths where the  $GdPO_4$  composition is at the border between the two structural modifications and, depending on the synthetic conditions used, can crystallize in either polymorph.

The synthesis of rhabdophane has been described in detail in the literature, focusing on hydrothermal (15) and microwave synthesis routes of rhabdophane, primarily for optical applications (17, 18). Typically, these reactions use  $LnCl_3 \cdot nH_2O$ ,  $Ln(NO_3)_3$ , and  $NH_4H_2PO_4$  or  $H_3PO_4$  as starting materials to obtain nanorods that are ~10 nm in size. Larger crystallites of rhabdophane can readily be synthesized using a hydrothermal route by combining  $LnCl_3$  with  $H_3PO_4$  and holding the mixture at 100° to 150°C for multiple days (14, 19),

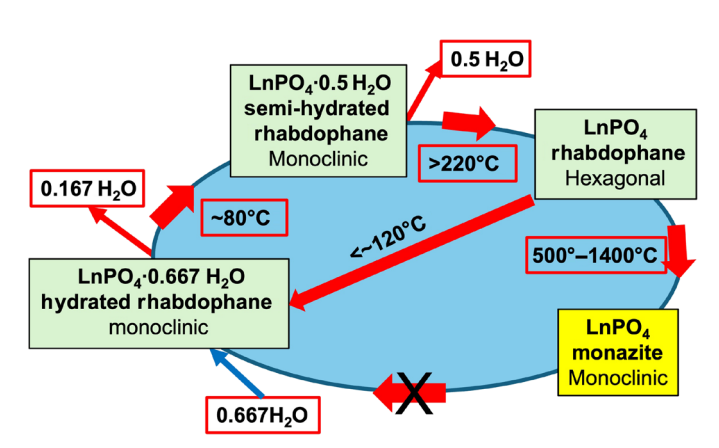


**Fig. 1. Schematic of rhabdophane to monazite conversion.** Heating the monoclinic hydrated phase of rhabdophane leads to water loss and transformation to the anhydrous hexagonal rhabdophane structure. This phase can rehydrate and revert to the monoclinic hydrated rhabdophane phase. Heating the hexagonal rhabdophane to temperatures near 1000°C leads to the irreversible conversion to the anhydrous monoclinic monazite phase. [Modified after Neumeier *et al.* (8)].

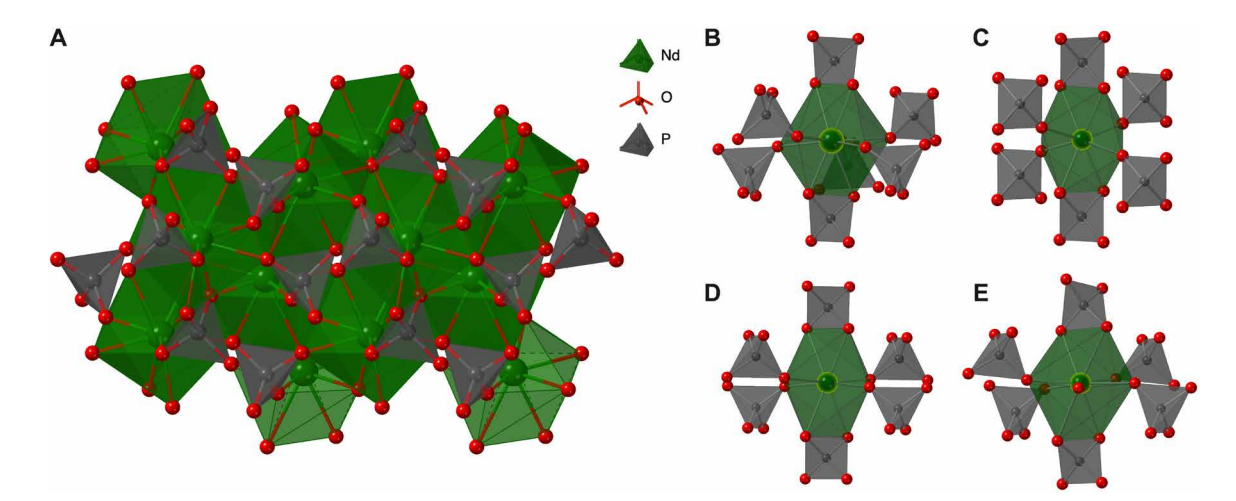


Fig. 2. Crystal structure of monazite and local coordination environments of monazite, xenotime, and rhabdophane. (A) Crystal structure of LnPO<sub>4</sub> monazite. PO<sub>4</sub>-tetrahedra, gray; LnO<sub>9</sub> polyhedra, dark green; O, red. Coordination environment of the central atom in (B) monazite and (C) xenotime and the two coordination environments in the (D) anhydrous and (E) hydrated rhabdophane structure. Green, central atom; gray, PO<sub>4</sub>; red, oxygen.

which may not be cost effective for a large-scale operation processing nuclear waste (9). As shown in Fig. 1, rhabdophane ( $LnPO_4 \cdot 0.67H_2O$ ) undergoes a sequential water loss starting at 80°C to form the hemihydrate and further loss starting at 220°C to form the anhydrous, hexagonal rhabdophane. This phase can rehydrate, and hence, it is necessary to thermally convert it to the denser monoclinic monazite structure, which is an irreversible structure transformation (20); the monoclinic monazite structure does not hydrate.

Here, we describe the low-temperature synthesis of rhabdophane and grayite and their respective low-temperature, acid-promoted conversion to monazite and cheralite, as well as the direct low-temperature synthesis of monazite and cheralite, including the pH dependence of their formation. Furthermore, we present a successful crystal growth approach and the resultant single-crystal structures of NdPO<sub>4</sub>,  $Ca_{0.5}Th_{0.5}PO_4$ , and  $Sr_{0.5}Th_{0.5}PO_4$  via a high-temperature flux route. Last, an in situ x-ray diffraction (XRD) hydrothermal study is described that allows us to propose a mechanism for the rhabdophane to monazite structural transformation.

### **RESULTS AND DISCUSSION**

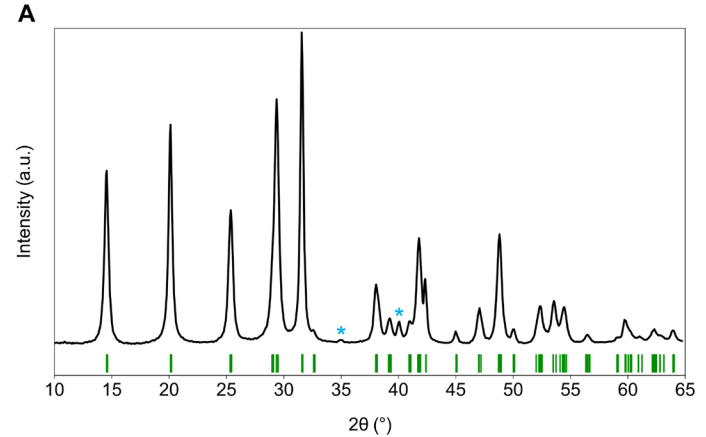
To accelerate the process of forming rhabdophane, we pursued a microwave-assisted method using a mixture of  $Ln_2O_3 + H_3PO_4$  that resulted in phase-pure rhabdophane in only 30 min in a microwave reactor at 100°C, producing highly crystalline rhabdophane samples (Fig. 3A). Heating the rhabdophane sample prepared via the microwave method in air to high temperatures (800° to 1400°C) results in complete dehydration and a structure conversion to the stable monazite phase (Fig. 3B). Depending on the temperature used, the crystallization takes less than 30 min to over 12 hours (table S2 and fig. S1).

Numerous studies have been performed on the conversion of rhabdophane to monazite, all generally using high temperatures (800° to 1400°C) to achieve the structural transformation. A recent paper by Enikeeva *et al.* (21) found that it was possible to convert nanosized rhabdophane to nanosized monazite under hydrothermal conditions in a conventional or microwave oven at much lower temperatures and earlier work by du Fou de Kerdaniel *et al.* (22) indicates the ability to use precipitation to obtain rhabdophane and monazite phases after a few hours to several months, with yields

ranging from 60 to 84% for the trivalent elements. The authors heated a mixture of  $La(NO_3)_3 \cdot 6H_2O$  and  $NH_4H_2PO_4$  in an autoclave to 210°C and studied the effect of time on product composition and particle size. They observed the initial formation of nanocrystalline rhabdophane that converted to nanocrystalline monazite upon longer heating. We have expanded upon this work by studying the effect of pH on the formation of monazite and by extending the synthesis technique to other lanthanides (Ln = Ce-Gd) and cheralite.

The CEM Discover 2.0 Microwave Synthesis System is capable of creating and maintaining hydrothermal reaction conditions to 300°C, allowing us to prepare the rhabdophane compositions at 100°C followed by a second heating cycle to temperatures in excess of 210°C to prepare polycrystalline monazite-type materials. Either heating  $Ln_2O_3 + H_3PO_4$  at low temperatures in a first step to prepare rhabdophane (fig. S2) and, in a second step, heating at 210° to 260°C to transform the rhabdophane to monazite or heating  $Ln_2O_3 + H_3PO_4$  in a single step to 210° to 260°C directly creates phase-pure monoclinic monazite as shown in (Fig. 4A). We observed that as the rare-earth ionic radii decrease, higher temperatures are needed to achieve the monazite phase. This aligns with the findings of du Fou de Kerdaniel et al. (22), who reported similar results using over-saturation processes to prepare phosphate ceramics. In addition, the use of higher synthesis temperatures, 260°C versus 210°C, results in sharper diffraction peaks (Fig. 4B), most evident for the peaks around 42° 2θ.

The crystallinity of the monazite product, as determined by the change in the peak width in the powder XRD (PXRD) pattern, can be enhanced by increasing the time of microwave heating as shown in Fig. 5, approaching the extremely high crystallinity observed upon heating these samples to 1200°C. Based on PXRD, it is evident that prolonged heating at temperatures ranging from 210° to 260°C improves the crystallinity. To establish the material origin of this change in crystallinity, we collected transmission electron microscopy (TEM) data. Bright-field images were taken from the samples treated at 210°C for 1 and 24 hours. A clear difference is visible between the morphologies of the particles at these two conditions (Fig. 6). A 1 hour treatment results in particles that are mostly thin needles a few 10 nm in width and 100 to 500 nm in length (Fig. 6A). The few seemingly wider particles consist of several agglomerated needles. The prolonged heating of 24 hours results in more isotropic



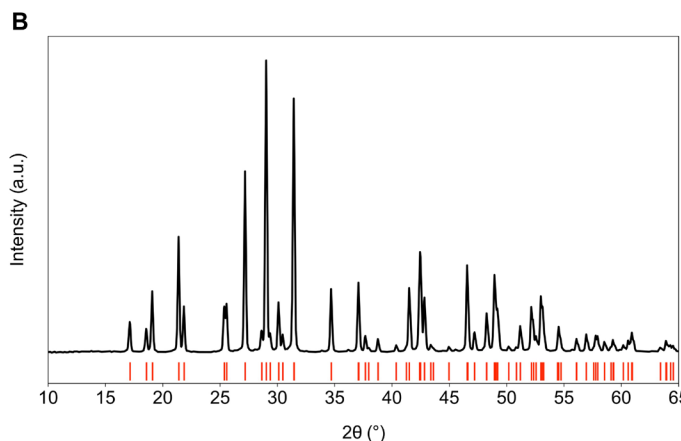


Fig. 3. Powder XRD patterns of NdPO<sub>4</sub>•nH<sub>2</sub>O (rhabdophane) and NdPO<sub>4</sub> (monazite). (A) Powder XRD (PXRD) pattern of NdPO<sub>4</sub>•nH<sub>2</sub>O (rhabdophane) prepared via microwave synthesis in 30 min at 100°C. Rhabdophane phase markers shown in green. Titanium peaks from the sample holder are marked with a blue \*. (B) PXRD pattern of the same sample after heating to 1200°C to transform the sample to NdPO<sub>4</sub> (monazite). Monazite phase markers shown in red.

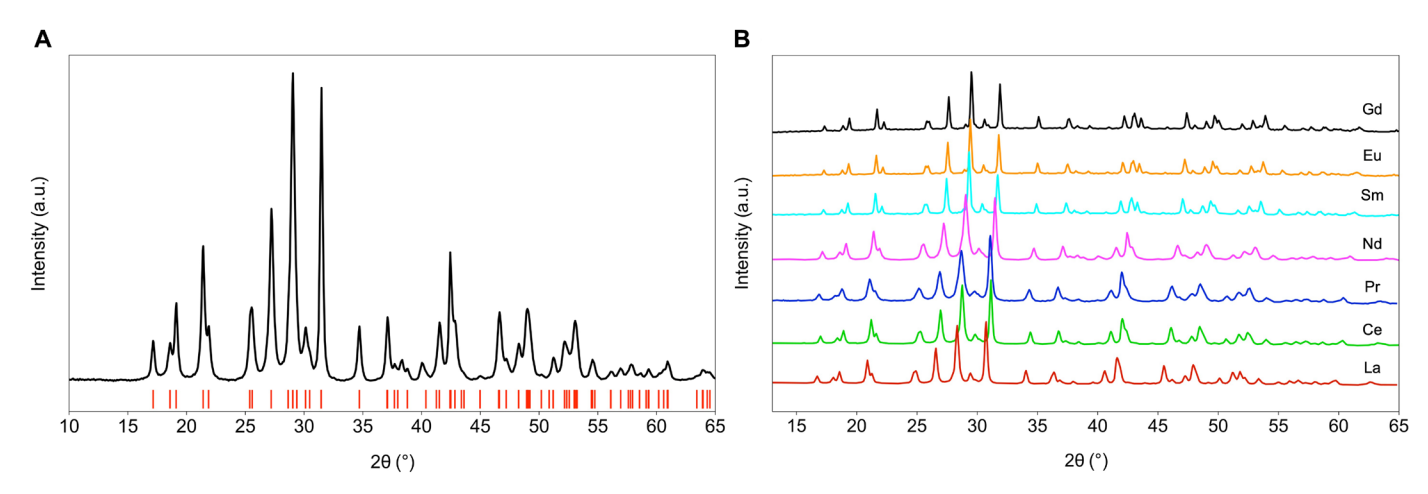


Fig. 4. PXRD patterns of microwave-synthesized monazite *LnPO*<sub>4</sub> [La-Nd, Sm-Gd]. (A) PXRD of monazite-NdPO<sub>4</sub> prepared by microwave processing at 210°C for 1 hour. Red lines represent the allowed Bragg reflections. (B) PXRD patterns of monazite-*LnPO*<sub>4</sub> [La-Nd, Sm-Gd] prepared by treating rhabdophane-*LnPO*<sub>4</sub> in H<sub>3</sub>PO<sub>4</sub> (1 M) at 210°C [La-Nd], 230°C [Sm], or 260°C [Eu-Gd] for 1 hour.

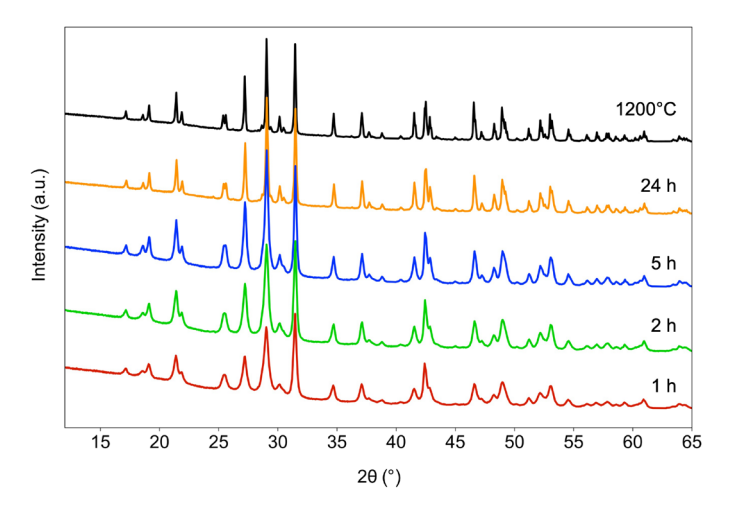


Fig. 5. PXRD patterns of NdPO<sub>4</sub> monazite prepared using different microwave heating times. Microwave synthesized monazite-NdPO<sub>4</sub> prepared using different heating times at 210°C in H<sub>3</sub>PO<sub>4</sub> (1 M) and, for comparison, a NdPO<sub>4</sub>•nH<sub>2</sub>O (rhabdophane) sample after heating to 1200°C for 0.5 hours.

particles with diameters ranging from 50 nm to a few hundred nanometers. Elongated particles are still present, but with significantly lower aspect ratio. This change in morphology agrees with the XRD results that show increased sharpness of the peaks upon longer heat treatments.

To investigate the unexpected low-temperature structural transformation further and to determine, among other considerations, if phosphoric acid is necessary to transform rhabdophane to monazite, several experiments were performed. First, microwave heating of rhabdophane in water at 210° to 260°C was carried out which, however, did not result in the full conversion of rhabdophane to monazite. To establish whether acidic conditions were needed for the transformation, 1 M  $\rm H_3PO_4$  was added and the mixture heated to 210° to 260°C, which resulted in the complete transformation to monazite. Clearly, the acidity plays a role. Last, to establish the impact of the pH value on the structure transformation, a series of reactions were performed using identical temperature and heating

times but varying different pH conditions. As seen in Fig. 7, the structure transformation goes to completion most quickly at low pH but does not reach complete conversion at neutral pH and does not convert at all under basic conditions. This implies that the pH (hydronium ions) is important in the mechanism of the transformation.

This approach can be extended from monazite to cheralite by performing the reaction with a divalent alkaline earth metal cation, such as Ca<sup>2+</sup> or Sr<sup>2+</sup>, and a tetravalent cation, such as Th<sup>4+</sup>, instead of a trivalent lanthanide. Bulk samples of Ca<sub>0.5</sub>Th<sub>0.5</sub>PO<sub>4</sub>/Sr<sub>0.5</sub>Th<sub>0.5</sub>PO<sub>4</sub> were obtained by using Th(NO<sub>3</sub>)<sub>4</sub>, (NH<sub>4</sub>)<sub>2</sub>HPO<sub>4</sub>, and Ca(NO<sub>3</sub>)<sub>2</sub>/ Sr(NO<sub>3</sub>)<sub>2</sub> as starting material and reacting them via microwave heating at 220°C in nitric acid (10<sup>-1</sup> to 10<sup>-6</sup> M) for 1 hour. Under highly acidic conditions, 1 M HNO<sub>3</sub>, Th<sub>2</sub>(HPO<sub>4</sub>)(PO<sub>4</sub>)<sub>2</sub>(H<sub>2</sub>O) is obtained. Reducing the acidity by using 0.1 M HNO<sub>3</sub>, a mixture of  $Ca_0$ ,  $Th_0$ ,  $PO_4$ ,  $Th_2(HPO_4)(PO_4)_2(H_2O)$ , and  $Th(PO_4)_4$  was obtained. The Ca<sub>0.5</sub>Th<sub>0.5</sub>PO<sub>4</sub> and a small quantity of an unknown impurities were obtained by using  $10^{-2}$  to  $10^{-6}$  M HNO<sub>3</sub> (fig. S3). The product obtained by using  $10^{-2}$  M HNO<sub>3</sub> was heated to 1000°, 1200°, and 1400°C for 0.5 hours, respectively, resulted in the formation of Ca<sub>0.5</sub>Th<sub>0.5</sub>PO<sub>4</sub> (fig. S4). Further optimization of the reaction conditions is being investigated.

### In situ XRD: Rhabdophane to monazite transition

To better understand the structural transformation between rhabdophane and monazite, we performed in situ PXRD (Fig. 8). Rhabdophane powder, presynthesized via microwave heating, was inserted into a fused silica capillary to which 1 M H<sub>3</sub>PO<sub>4</sub> was added as the hydrothermal reaction medium. Heating from room temperature to 210°C, we observe the diffraction lines for rhabdophane up to about 165°C. Over a temperature range of about 15°, the diffraction lines disappear, and during that same temperature range, the diffraction lines for monazite appear; no intermediate phase can be seen. The crystallinity of the monazite increases during heating to 210°C. Further heating at 210°C for 5 hours did not noticeably increase the sharpness of the diffraction lines.

This low-temperature conversion can be contrasted with the thermal conversion of rhabdophane to monazite (fig. S5). Heating the same rhabdophane material as was used in the hydrothermal process in a hot stage in air reveals the transition from rhabdophane to monazite at

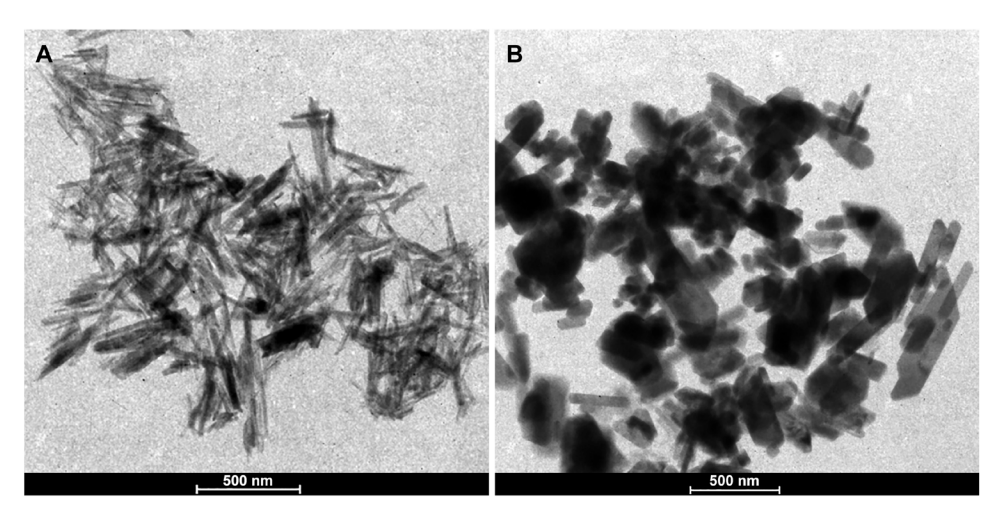
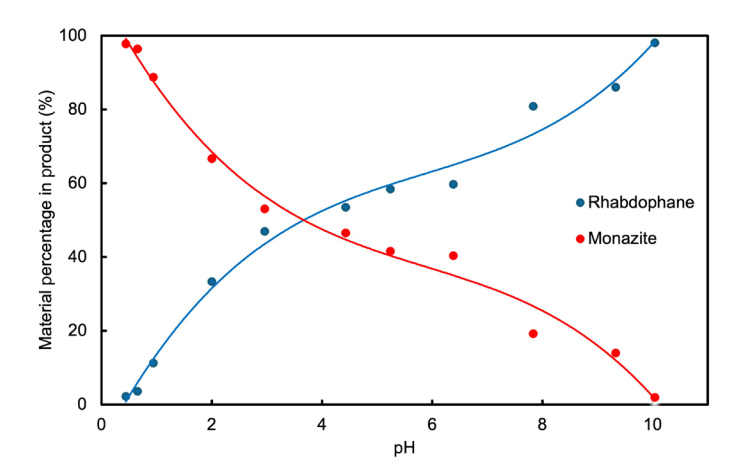


Fig. 6. Change in crystallinity of NdPO<sub>4</sub> (monazite) prepared via microwave synthesis for 1 and 24 hours. (A) Bright-field TEM image of NdPO<sub>4</sub> treated at 210°C for 1 hour. (B) NdPO<sub>4</sub> treated at 210°C for 24 hours.



**Fig. 7. pH dependence of the monazite formation in microwave synthesis.** Rhabdophane and monazite phase percentages after synthesis at different pH reaction conditions, where the lines are added to guide the eye.

700° to 800°C. An earlier phase transition at 200°C is due to the dehydration of rhabdophane (fig. S6). Clearly, the hydrothermal structure transition of rhabdophane to monazite is not purely thermally driven.

To help understand the process of the structure conversion, we can look at zeolites, some of which are known to undergo a structure transformation under hydrothermal conditions. Norby (23) studied the hydrothermal conversion of zeolite LTA using LiCl(aq) to zeolite Li-A(BW) using in situ synchrotron diffraction measurements. The synchrotron data also exhibited the simultaneous presence of diffraction lines belonging to both phases during the structure transition. Norby (23) considered several mechanisms for the structure transformation, including an internal structure transformation, a solution mediated transformation, and a surface mediated transformation. On the basis of an analysis of the kinetics of the phase transformation and an scanning electron microscopy (SEM) analysis of particles generated during ex situ reactions, Norby (23) concluded that for this zeolite system the solution mediated mechanism was the most likely, with only very small amounts of the aluminosilicate

in solution. Garcia-Martinez *et al.* (24) recently investigated the hydrothermal transformation of Faujasite (FAU) to beta-zeolite (BEA). The authors analyzed the interzeolite transformation and found that FAU completely loses its crystallinity before BEA starts to form. This structure transformation via an amorphous precursor was postulated to occur via a liquid phase–mediated mechanism, where the authors believed that the base causes amorphization and partial dissolution, followed by reconstitution of the BEA structure.

In the case of the rhabdophane to monazite transformation, a thermal transformation does not occur at reasonable rates below 800°C, suggesting that the observed transformation at ~165°C is not simply be a thermal process. Furthermore, we do not observe the disappearance of the initial rhabdophane phase followed by the appearance of the monazite phase but rather observe the coexistence of both phases over a 15°C temperature window, ruling out a complete dissolution-recrystallization mechanism. This is supported by the reported solubility of rhabdophane, which is very low at pH = 1 and 298 to 343 K, with logK°<sub>s,0</sub> ranging from -25 to -26 (25). For our system, the process is pH dependent and proceeds best at very low pH values, where the solubility of rhabdophane is very low, which would not favor a dissolution-recrystallization mechanism. Nonetheless, we cannot rule out either solution-mediated dissolution-recrystallization mechanism or an internal structure transformation.

The channels of the rhabdophane structure contain water in the hydrated form. Therefore, it is possible that the oxygens lining the channels of the hexagonal rhabdophane structure (Fig. 9) become protonated under the low pH reaction conditions, weakening the polyhedral connectivity. The monazite (monoclinic) and rhabdophane (monoclinic) structures share very similar structural units, such as the chains of alternating metal (green) and phosphate (gray) polyhedra. These chains (in both structure depictions they run into the page) are connected lateral to each other via O—*Ln* bonds. One can hypothesize that a protonation of oxygens involved in the O—*Ln* bonds of the hexagonal rhabdophane structure could lead to a weakening of the lateral bonding connections and allow the chains to evolve into the denser monazite structure, which would be considered an internal structure rearrangement; however, the exact mechanism remains to be determined.

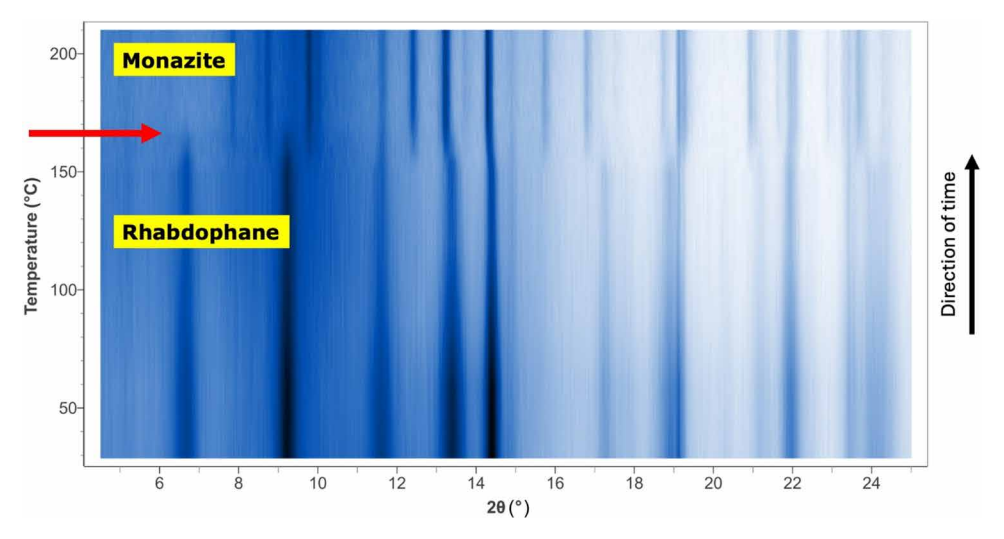


Fig. 8. Hydrothermal conversion of NdPO<sub>4</sub>-nH<sub>2</sub>O rhabdophane to monoclinic NdPO<sub>4</sub> monazite monitored by in situ PXRD. PXRD data of the in situ hydrothermal conversion of rhabdophane, NdPO<sub>4</sub>-nH<sub>2</sub>O, to monoclinic monazite, NdPO<sub>4</sub>, in 1 M H<sub>3</sub>PO<sub>4</sub>. The rhabdophane sample and 1 M phosphoric acid were sealed inside a capillary tube and heated from room temperature to 220°C inside the furnace attachment to the powder diffractometer. The phase transition of the presynthesized rhabdophane phase to the monoclinic monazite phase ( $\sim$ 165° to 180°C) can be seen in the waterfall plot that covers the temperature range of 30° to 220°C.

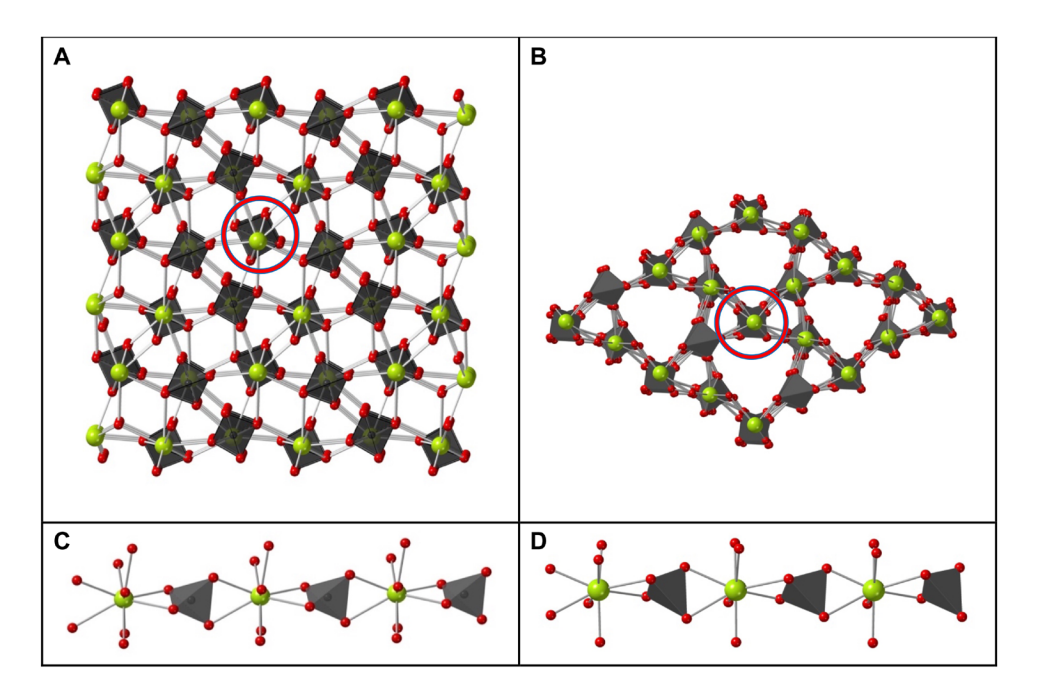


Fig. 9. Illustration of the crystal structures and similarity of the chains of alternating rare-earth and phosphate polyhedra in monazite and rhabdophane.

(A) Crystal structure of monazite. (B) Crystal structure of rhabdophane. (C) Illustration of the alternating rare-earth and phosphate polyhedra chain in monazite.

(D) Illustration of the alternating rare-earth and phosphate polyhedra chain in rhabdophane.

# **Chemical durability**

Accelerated aqueous leach testing of powders of NdPO $_4$  was carried out to assess their chemical durability. The measured concentration of Nd in the leachates was <1.5 µg/liter, the detection limits of the methods used. The measured concentration of P in the leachates was ~3 to 9 mg/liter, which was used to compute a normalized loss (NLP) of ~7.2  $\times$  10 $^{-5}$  g/m $^2$  for sintered samples and ~2.2  $\times$  10 $^{-4}$  g/m $^2$  for microwave samples. Leach tests were carried out in triplicate alongside

the approved reference material (ARM-1) (26), which were within acceptable control chart values for normalized B release, the HLW benchmark value.

These leach tests were conducted at a significantly higher surface area to volume ratios than nominally described in standard leach tests for HLW glasses. It is known that exposed surface area, in combination with the other test parameters, has a significant influence on the leachate chemistry and subsequent analysis (27). In particular,

actinide series and other +3 elements can adhere to the vessel walls used during leach testing. Therefore, acid stripping and subsequent analysis can be performed to ensure mass balance of the material losses. Acid strip was not conducted here, but it is noted that the pH of the leachate solutions at the completion of the test were low pH, between 3.1 and 3.9. Although the powders were washed, the pH change during the leach testing is attributed to phosphate, which is evidenced in the chemical analysis and may also be from residual reagents/reactions during the synthesis. If the measured P in the leachate is residual, then the mass fraction of Nd loss, computed at the detection limit, would be ~0.008 weight % (wt %) of the initial mass of the powder(s). However, if Nd and P are assumed to leach stoichiometrically, then the estimated fraction of Nd loss would be ~0.2 to 0.7 wt %, depending on the synthetic method. Together, these test results indicate the excellent chemical durability of the NdPO<sub>4</sub> phase and by extension its transuranic analogs.

### **Crystal growth**

The ability to grow crystals of target phases can greatly help in enhancing our understanding of their crystal structures, and furthermore, these structure solutions provide us with precise atomic positions and bond lengths (28-36) that can be used for Rietveld refinements. Our group has pursued high-temperature flux crystal growth of mixed metal phosphate compositions in the past and has been very successful in obtaining compositions of the type  $A_3Ln(PO_4)_2$  (A = alkali metals) using an alkali chloride/alkali fluoride flux (30). For a preliminary exploration of the crystal growth of monazite phases, we used several fluxes, including the Na<sub>2</sub>CO<sub>3</sub>/MoO<sub>3</sub> flux first published by Cherniak et al. (37) that, however, requires a presynthesized monazite powder. To improve upon this and to develop a more convenient method, we decided to start with oxides and nitrates of the rare earths together with (NH<sub>4</sub>)<sub>2</sub>HPO<sub>4</sub> as the phosphate source and a CsCl/CsF flux. As shown in Fig. 10, our results demonstrate that both approaches result in high-quality crystals. Other fluxes that are very successful include Pb<sub>2</sub>PO<sub>7</sub> (11); however, because of the presence of lead coupled with its poor water solubility that makes flux removal difficult, Pb<sub>2</sub>PO<sub>7</sub> is significantly less ideal to use than ACl/AF or A<sub>2</sub>O/  $MoO_3$  (A = alkali metal).

Crystals of NdPO<sub>4</sub> have been grown by Cherniak *et al.* (37); however, no reports of single crystal structure solutions of Ca<sub>0.5</sub> Th<sub>0.5</sub>PO<sub>4</sub> and Sr<sub>0.5</sub>Th<sub>0.5</sub>PO<sub>4</sub> can be found in the literature. A paper by Podor *et al.* (38) reports the supercritical hydrothermal synthesis of Ca<sub>0.5</sub>Th<sub>0.5</sub>PO<sub>4</sub> crystals, but only unit cells from PXRD data are reported. The alkaline earth cation and the thorium cation occupy the same crystallographic site in a 50:50 ratio to achieve charge balance with the phosphate groups. The structure can be thought of as a monazite with Ca/Th or Sr/Th occupying the rare-earth site.

The ability to perform the low-temperature synthesis of monazite via the described acid-promoted structure transformation between the rhabdophane and the monazite phase starting at ~165°C demonstrates the feasibility of creating a waste form for containing the actinides (Np, Pu, Am, and Cm). The monazite phase readily achieves this via the ability to create both  $Ln(III)PO_4$  and  $M(II)/Th(IV)PO_4$ , allowing this family of phosphates to be used as a durable waste form with high waste element loading that can help in the sequestration of existing and future high-level nuclear waste.

### **MATERIALS AND METHODS**

### Reagents

La<sub>2</sub>O<sub>3</sub> (99.9%; Alfa Aesar), Ce(NO<sub>3</sub>)<sub>3</sub>·6H<sub>2</sub>O (99.9%; BTC), Pr(NO<sub>3</sub>)<sub>3</sub>·6H<sub>2</sub>O (99.9%; Acros), Sm<sub>2</sub>O<sub>3</sub> (99.9%; Alfa Aesar), Eu<sub>2</sub>O<sub>3</sub> (99.9%; Alfa Aesar), Gd<sub>2</sub>O<sub>3</sub> (99.9%; Alfa Aesar), Th(NO<sub>3</sub>)<sub>4</sub>·4H<sub>2</sub>O (JT Baker, NA), Ca(NO<sub>3</sub>)<sub>2</sub>·4H<sub>2</sub>O (99.5%; Thermo Fisher Scientific), NH<sub>4</sub>H<sub>2</sub>PO<sub>4</sub> (99.9%; Sigma-Aldrich), (NH<sub>4</sub>)<sub>2</sub>HPO<sub>4</sub> (VWR), Li<sub>2</sub>CO<sub>3</sub> (Mallinckrodt), Na<sub>2</sub>CO<sub>3</sub> (Thermo Fisher Scientific), MoO<sub>3</sub> (99.9%; Strem), CsCl (VWR, ultrapure), CsF (99.0%; Alfa Aesar), LaF<sub>3</sub> (99.0%; Thermo Fisher Scientific), LaCl<sub>3</sub> (99.9%; Alfa Aesar), hydrochloric acid (Thermo Fisher Scientific), and phosphoric acid (Thermo Fisher Scientific, 85%) were used as received. Nd<sub>2</sub>O<sub>3</sub> (99.9%; Alfa Aesar) had transformed to the hydroxide [Nd(OH)<sub>3</sub>] due to moisture absorption and was used as such.

### Microwave-assisted reaction

The CEM Discover 2.0 Microwave Synthesizer, equipped with an infrared temperature sensor and advanced vent-and-reseal technology,

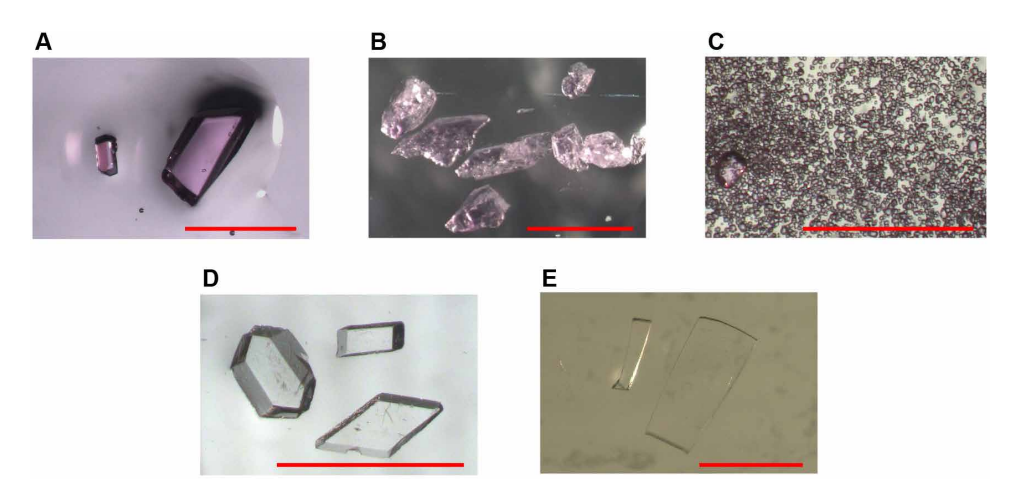


Fig. 10. Morphology and colors of flux grown monazite and cheralite single crystals. (A) NdPO<sub>4</sub> crystals grown in Na<sub>2</sub>CO<sub>3</sub>/MoO<sub>3</sub>. (B) NdPO<sub>4</sub> crystals grown in CsCl/CsF fluxes. (C) Phase-pure NdPO<sub>4</sub> crystals grown in Li<sub>2</sub>CO<sub>3</sub>/MoO<sub>3</sub>. (D) Ca<sub>0.5</sub>Th<sub>0.5</sub>PO<sub>4</sub> crystals grown in Li<sub>2</sub>CO<sub>3</sub>/MoO<sub>3</sub>. (E) Sr<sub>0.5</sub>Th<sub>0.5</sub>PO<sub>4</sub> crystals grown in Li<sub>2</sub>CO<sub>3</sub>/MoO<sub>3</sub>. Scale bars, 1 mm.

was used to prepare bulk products. It features a 300-ml single-mode microwave cavity and is fully programmable.

Rhabdophane- $LnPO_4$  (La-Nd, Sm-Gd) and monazite- $LnPO_4$  (La-Nd, Sm-Gd) were obtained as bulk products by performing hydrothermal reactions in the microwave-assisted heating system.  $Ln_2O_3/Ln(NO_3)_3/Ln(OH)_3$  were combined in a 35-ml Pyrex tube, to which diluted  $H_3PO_4$  (1 M, 8 ml) was added. The tube was placed into the microwave system and heated under stirring to the selected temperatures. Rhabdophane- $LnPO_4$  (La-Nd, Sm-Eu) was obtained after heating at 100°C for 30 min. Phase-pure GdPO $_4$  was obtained after heating at 180°C for 30 min. Monazite- $LnPO_4$  (Ln = La-Nd, Sm-Gd) is obtained by heating either the starting materials or presynthesized rhabdophane- $LnPO_4$  (La-Nd/Sm/Eu-Gd) at 210°/230°/260°C for an hour, respectively. Monazite- $LnPO_4$  can also be prepared starting with either  $LnCl_3$  or  $LnF_3$  by reacting with  $H_3PO_4$  (1 M, 8 ml) at 230°C for 1 hour (fig. S7). All products were collected by filtration and washed with water and acetone.

Cheralites,  $Ca_{0.5}Th_{0.5}PO_4$  and  $Sr_{0.5}Th_{0.5}PO_4$ , were obtained by using  $Th(NO_3)_4$  (0.2 mmol),  $Ca(NO_3)_2/Sr(NO_3)_2$  (0.2 mmol), and  $(NH_4)_2HPO_4$  (0.4 mmol) as starting materials as well as 4 ml of  $10^{-1}$  M- $10^{-6}$  M HNO $_3$ /water as the solvent, reacted at 220°C for 1 hour via microwave heating (figs. S3 and S8). All products were collected by filtration and washed with water and methanol.

To investigate the impact of time and pH on the structure transformation, the following reactions were performed in the microwave system: The rhabdophane-NdPO<sub>4</sub> was placed into a 35-ml Pyrex tube with phosphoric acid (1 M), sealed by a plastic cap, placed into the microwave, and heated to 210°C. The slurries were kept at 210°C for 1, 2, and 5 hours. The products were isolated via filtration and structurally characterized by Rietveld refinement. The phase transformation from rhabdophane-NdPO<sub>4</sub> to monazite-NdPO<sub>4</sub> was studied in hydrochloric acid using different concentrations. A 1 M HCl was diluted by adding distilled water, and the pH was measured by using a digital pH meter. For each reaction, 100 mg of rhabdophane-NdPO4 was placed into a 10-ml Pyrex tube with 2 ml of hydrochloric acid, sealed by a plastic cap, placed into the microwave, and heated to 210°C. The slurries were kept at 210°C for 1 hour in the microwave heating system and then structurally characterized by Rietveld refinement.

# Flux reaction

# Monazite crystal growth using monazite precursor powder

The rhabdophane-NdPO<sub>4</sub> obtained by microwave synthesis was dried at 200°C overnight followed by heating for 1 hour at 500°C, followed by 1 hour at 800°C in an alumina crucible. The thus prepared monazite powder was placed into a covered platinum crucible containing either Na<sub>2</sub>CO<sub>3</sub>/MoO<sub>3</sub> or Li<sub>2</sub>CO<sub>3</sub>/MoO<sub>3</sub> as the flux. The molar ratio of phosphate to carbonate to MoO<sub>3</sub> used was 1:5:15. The mixture was held at 1000°C for 24 hours, cooled at 3°C/hour to 750°C, and subsequently cooled to room temperature by turning off the furnace. Single crystals of NdPO<sub>4</sub> were isolated from the residual flux by sonicating in distilled water and collected by vacuum filtration.

### Monazite crystal growth from precursor reagents

Single crystals of monazite-NdPO<sub>4</sub> can also be obtained in a one-step crystal growth reaction by using (i) Li<sub>2</sub>CO<sub>3</sub>/MoO<sub>3</sub> or (ii) CsCl/CsF as the flux. (i) Nd(OH)<sub>3</sub> (0.2 mmol, 33.6 mg) and NH<sub>4</sub>H<sub>2</sub>PO<sub>4</sub> (0.2 mmol, 23.0 mg) were reacted in a Li<sub>2</sub>CO<sub>3</sub> (0.4 mmol, 29.6 mg) and MoO<sub>3</sub> (1.2 mmol, 172.7 mg) flux. The mixture was held at 1000°C

for 24 hours, then cooled at 3°C/hour to 750°C, and subsequently cooled to room temperature by turning off the furnace. Phase-pure single crystals of NdPO<sub>4</sub> were isolated after removing any residual flux by sonicating in distilled water (fig. S9). (ii) Nd(OH)<sub>3</sub> (1 mmol, 195 mg), (NH<sub>4</sub>)<sub>2</sub>HPO<sub>4</sub> (1 mmol, 132 mg), CsCl (11 mmol, 1.85 g), and CsF (9 mmol, 1.37 g) were mixed and added to a platinum crucible. The mixture was held at 875°C for 12 hours, cooled at 6°C/hour to 400°C, and lastly allowed to cool to room temperature after turning off the furnace. Large (>2 mm) single crystals of NdPO<sub>4</sub> were isolated from the flux via sonication in deionized water followed by suction filtration.

The single crystals of cheralite-type  $Ca_{0.5}Th_{0.5}PO_4$  and monazite-type  $Sr_{0.5}Th_{0.5}PO_4$  were obtained by a modified one-step flux reaction.  $Th(NO_3)_4\cdot 4H_2O$ ,  $Ca(NO_3)_2\cdot 4H_2O$  or  $Sr(NO_3)_2$  and  $(NH_4)_2HPO_4$  (1.0 mmol, 132.0 mg) were mixed in a 1:1:2 molar ratio and combined with the flux consisting of  $Li_2CO_3$  and  $MoO_3$  in a 1:3 molar ratio. The mixture was held at  $1000^{\circ}C$  for 24 hours, cooled at  $3^{\circ}C$ /hour to  $750^{\circ}C$ , and subsequently cooled to room temperature by turning off the furnace. The crystals were isolated from the residual flux by sonicating in distilled water followed by vacuum filtration.

### **Structure determination**

X-ray intensity data were collected at room temperature using a Bruker D8 QUEST diffractometer equipped with a PHOTON-II area detector and an Incoatec microfocus source (Mo K $\alpha$  radiation,  $\lambda=0.71073$  Å). The crystals were mounted on a microloop using immersion oil. The raw area detector data frames were reduced and corrected for absorption effects using the SAINT+ and SADABS programs. Final unit cell parameters were determined by least-squares refinement. Initial structural models were obtained with SHELXT. Subsequent difference Fourier calculations and full-matrix least-squares refinement against  $F^2$  were performed with SHELXL-2018 using Olex2 (39–43). The crystallographic data and results of the diffraction experiments are summarized in table S3.

# Powder XRD

PXRD data for all phases were collected on a Bruker D2 powder x-ray diffractometer with Cu K $\alpha$  radiation (30 kV, 10 mA,  $\lambda$  = 1.5418 Å) between 5.0° and 65.0° 2 $\theta$ .

# **Thermal properties**

Thermogravimetric analysis measurements were performed on rhabdophane-NdPO<sub>4</sub> using a TA Instruments SDT Q600. The sample was heated at  $10^{\circ}$ C/min to  $1200^{\circ}$ C and then cooled at  $10^{\circ}$ C/min to  $100^{\circ}$ C (fig. S6).

### Transmission electron microscopy

For the TEM studies, the powder samples were dispersed in ethanol without crushing. Then, a few drops of this solution were deposited on copper grids covered with holey carbon to be used as TEM samples. Bright-field images of these TEM samples were taken at a Thermo Fisher Tecnai G2 transmission electron microscope operated at 200 kV. Contrast was enhanced by using the microscope's objective aperture that limits the resolution of the diffraction patterns to 1 Å.

# **Chemical durability**

Powder samples of NdPO<sub>4</sub> were tested in their as-prepared physical state. Powder prepared via the microwave assistance methodology was tested along with powder prepared using conventional furnace

heating for comparison. Aqueous leaching tests following the ASTM C1285 product consistency test method-B protocol was used to measure elemental release from the NdPO<sub>4</sub> phase. Before the leach testing, all samples were washed with water and alcohol and dried. Samples were measured alongside a reference (ARM-1) (26) in triplicate and two blanks. Tests were performed by combining ~10 ml of deionized water (leachant) with 0.2 to 0.3 g of sample/reference in sealed stainless-steel vessels at 90°  $\pm$  2°C for 7 days. Once cooled down to room temperature, the leachate solutions were sampled, acidified, and analyzed by ICP mass spectrometry for elemental concentrations. The Brunauer-Emmett-Teller surface area of the sample powders after leaching was measured using an ASAP 2020 (Micromeritics) instrument.

### Rietveld refinement

The Rietveld scans of selected samples were collected on a Rigaku Ultima IV powder x-ray diffractometer with Cu Kα radiation (40 kV, 44 mA,  $\lambda = 1.5418 \text{ Å}$ ) between 10° and 120° (20) in steps of 0.02°. The Rietveld scans of mixtures of rhabdophane and monazite phases obtained by pH study were collected on a Bruker D2 powder x-ray diffractometer with Cu K $\alpha$  radiation (30 kV, 10 mA,  $\lambda = 1.5406$  Å) between 5.0° and 95.0° 2θ. Rietveld refinements were performed using the Bruker TOPAS commercial v5 software in launch mode using jEdit (v4.3.1) with macros for TOPAS (44). The default approach consisted of refining the unit cell parameters, the Gaussian and Lorentzian isotropic size parameters, scale factors, and Chebyshev background parameters. Initial lattice parameters and atomic positions were taken from single-crystal structure solutions. The Rietveld plots were created using CrystalDiffract (figs. S10 to S26). The percentages of rhabdophane and monazite phase after synthesis at different pH reaction conditions were summarized in table S4. The atomic positions of selected samples were summarized in tables S5 to S10. The crystallographic data for the Rietveld structure refinement can be found in table S11.

## **Energy dispersive spectroscopy**

Crystals were mounted on an SEM stub with carbon tape. Energy dispersive spectroscopy (EDS) data of Ca<sub>0.5</sub>Th<sub>0.5</sub>PO<sub>4</sub> were collected using a Zeiss FESEM instrument equipped with a Thermo EDS attachment. The SEM was operated in low-vacuum mode with a 15-kV accelerating voltage and a 30-s accumulating time (fig. S27). EDS data of Sr<sub>0.5</sub>Th<sub>0.5</sub>PO<sub>4</sub> were collected using a Tescan Vega 3 SEM instrument equipped with a Thermo EDS attachment. The SEM was operated in low-vacuum mode with a 20-kV accelerating voltage and a 30-s accumulating time (fig. S28).

### In situ PXRD

Polycrystalline powder of rhabdophane-NdPO<sub>4</sub> and 1 M phosphoric acid were loaded into a fused silica capillary (1 mm outer diameter, 0.8 mm inner diamter) which was then frozen using liquid nitrogen. A micro-torch using a MAPP (methylacetylene, propadiene, and propane)/oxygen mixture was then used to seal the capillary with a final length of approximately 2.5 cm. This airtight capillary was then inserted into the end of a thin and hollow copper pipe (7.25-cm long, 2.4-mm outer diameter) with the portion of the capillary intended for measurement protruding from the end (fig. S29). The capillary was held in place inside the copper pipe with modeling clay. The now-extended capillary was then inserted into a rotating capillary attachment of an Anton Paar HTK 1200 N high-temperature oven,

controlled by an Anton Paar CCU 1000, attached to a Rigaku Smart-Lab X-ray Diffractometer equipped with a D/teX Ultra 250-HE high-resolution detector and rotating Mo ( $\lambda$  = 0.709 Å) anode operated at 45 kV and 200 mA (9 kW).

Variable temperature in situ XRD patterns were collected from the capillary using cross-beam (convergent) optics in Debye-Scherrer geometry from 4.5° to 25° 20 (d<sub>hkl</sub>  $\approx$  0.84 to 4.5 Å) at 1.6°/min. Temperatures were measured using a Pt10%Rh-Pt thermocouple (type S) with an accuracy of  $\pm 2^{\circ}\text{C}$ . Scans were performed at 30°C increments from 30° to 150°C, at 5°C increments from 150° to 210°C, and lastly every 15 min while holding at 210°C for an addition 11 hours.

### **Supplementary Materials**

This PDF file includes:

Tables S1 to S11 Figs. S1 to S29

### REFERENCES AND NOTES

- H.-C. zur Loye, T. M. Besmann, J. W. Amoroso, K. S. Brinkman, A. Grandjean, C. H. Henager, S. Hu, S. T. Misture, S. R. Phillpot, N. B. Shustova, H. Wang, R. J. Koch, G. Morrison, E. A. Dolgopolova, Novel approaches to hierarchical materials as tailored nuclear waste forms: A perspective. *Chem. Mater.* 30, 4475–4488 (2018).
- S. Park, R. C. Ewing, US legal and regulatory framework for nuclear waste from present to future reactors and their fuel cycles. Annu. Rev. Env. Resour. 48, 713–736 (2023).
- R. C. Ewing, Nuclear waste forms for actinides. Proc. Natl. Acad. Sci. U.S.A. 96, 3432–3439 (1999).
- J. Marra, A. Cozzi, C. Crawford, C. Herman, J. Marra, D. Peeler, Development Of Glass And Crystalline Ceramic Forms For Disposition Of Excess Plutonium 2009 International symposium on radiation safety management (OECD Nuclear Energy and IAEA, 2009), vol. 40, p. 00482.
- M. I. Ojovan, S. V. Yudintsev, Glass, ceramic, and glass-crystalline matrices for HLW immobilisation. Open Ceram. 14, 100355 (2023).
- National Research Council Glass as a Waste Form and Vitrification Technology: Summary of an International Workshop (The National Academies Press, 1996).
- A. E. Ringwood, S. E. Kesson, N. G. Ware, W. O. Hibberson, A. Major, The SYNROC process: A geochemical approach to nuclear waste immobilization. *Geochem. J.* 13, 141–165 (1979).
- S. Neumeier, Y. Arinicheva, Y. Ji, J. M. Heuser, P. M. Kowalski, P. Kegler, H. Schlenz, D. Bosbach, G. Deissmann, New insights into phosphate based materials for the immobilization of actinides. *Radiochem. Acta* 105, 961–984 (2017).
- N. Dacheux, N. Clavier, R. Podor, Monazite as a promising long-term radioactive waste matrix: Benefits of high-structural flexibility and chemical durability. Am. Mineral. 98, 933, 947 (2013)
- H. Schlenz, J. M. Heuser, A. Neumann, R. Schmitz, D. Bosbach, Monazite as a suitable actinide waste form. Z. Kristallogr. 228, 113–123 (2013).
- L. A. Boatner, Synthesis, structure, and properties of monazite, pretulite, and xenotime. Rev. Mineral. Geochem. 48, 97–121 (2002).
- M. R. Rafiuddin, G. Donato, S. McCaughertry, A. Mesbah, A. P. Grosvenor, Review of rare-earth phosphate materials for nuclear waste sequestration applications. ACS Omega. 7, 39482–39490 (2022).
- S. Chong, B. J. Riley, Z. J. Nelson, Crystalline compounds for remediation of rare-earth fission products: A review. J. Rare Earths. 40, 365–380 (2022).
- A. Mesbah, N. Clavier, E. Elkaim, S. Szenknect, N. Dacheux, In pursuit of the rhabdophane crystal structure: from the hydrated monoclinic LnPO<sub>4</sub>•0.667H<sub>2</sub>O to the hexagonal LnPO<sub>4</sub> (Ln = Nd, Sm, Gd, Eu and Dy). *J. Solid State Chem.* 249, 221–227 (2017).
- M. R. Rafiuddin, A. P. Grosvenor, A structural investigation of hydrous and anhydrous rare-earth phosphates. *Inorg. Chem.* 55, 9493–9950 (2016).
- S. Chong, B. J. Riley, X. Lu, J. Du, T. Mahadevan, V. Hedge, Synthesis and properties of anhydrous rare-earth phosphates, monazite and xenotime: a review. RSC Adv. 14, 18978–19000 (2024).
- M. T. Colomer, A. L. Ortiz, Effect of Tb<sup>3+</sup> doping and self generated pressure on the crystallographic/morphological features and thermal stability of LaPO<sub>4</sub>-nH<sub>2</sub>O single-crystal nanorods obtained by microwave assisted hydrothermal synthesis. Ceram. Int. 42, 18074–18086 (2016).
- C. R. Patra, G. Alexandra, S. Patra, D. Solomon, D. S. J. Gedanken, A. Landau, Y. Gofer, Microwave approach for the synthesis of rhabdophane-type lanthanide orthophosphate (Ln = La, Ce, Nd, Sm, Eu, Gd, and Tb) nanorods under solvothermal conditions. *New J. Chem.* 29, 733–739 (2003).

# SCIENCE ADVANCES | RESEARCH ARTICLE

- F. Shiba, T. Fujiwara, Y. Takeda, Y. Okawa, Formation and aspect ratio control of rhabdophane-type yttrium orthophosphate hexagonal prism particles synthesized by a citrate- assisted hydrothermal process. CrstEngComm 24, 2958–2965 (2022).
- A. Shelyug, A. Mesbah, S. Szenknect, N. Clavier, N. Dacheux, A. Navortsky, Thermodynamics and stability of rhabdophanes, hydrated rare earth phosphates REPO<sub>4\*</sub>nH<sub>2</sub>O. Front. Chem. 6, 604 (2018).
- M. O. Enikeeva, K. M. Kenges, O. V. Proskurina, D. P. Danilovich, V. V. Gusarov, Influence of hydrothermal treatment conditions on the formation of lanthanum orthophosphate nanoparticles of monazite structure. *J. Appl. Chem.* 93, 540–548 (2020).
- E. D. F. de Kerdaniel, N. Clavier, N. Dacheux, O. Terra, R. Podor, Actinide solubility-controlling phases during the dissolution of phosphate ceramics. J. Nucl. Mater. 362, 451–458 (2007).
- 23. P. Norby, Hydrothermal conversion of zeolites: An in situ synchrotron x-ray powder diffraction study. *J. Am. Chem. Soc.* **119**, 5215–5221 (1997).
- M. J. Mendoza-Castro, E. De Oliveira-Jardim, N.-T. Ramírez-Marquez, C.-A. Trujillo, N. Linares, J. García-Martínez, Hierarchical catalysts prepared by interzeolite transformation. J. Am. Chem. Soc. 144, 5163–5171 (2022).
- C. Gausse, S. Szenknect, D. W. Qin, A. Mesbah, N. Clavier, S. Neumeier, D. Bosbach, N. Dacheux, Determination of the Solubility of Rhabdophanes LnPO<sub>4</sub>•0.667H<sub>2</sub>O (Ln = La to Dy). Eur. J. Inorg. Chem. 2016, 46615–44630 (2016).
- G. B. Mellinger, J. L. Daniel, Approved Reference and Testing Materials for Use in Nuclear Waste Management Research and Development Programs (Pacific Northwest National Laboratory, 1984).
- W. L. Ebert , J. K. Bates, A Comparision of Glass Reaction at High and Low S/V: PCT vs. MCC-1 (Argonne National Lab, 1992).
- D. E. Bugaris, H.-C. zur Loye, Materials discovery by flux crystal growth: Quaternary and higher order oxides. *Angew. Chem. Int. Ed. Engl.* 51, 3780–3811 (2012).
- T. K. Deason, A. T. Hines, G. Morrison, M. D. Smith, T. M. Besmann, A. M. Mofrad, F. F. Fondeur, I. Lehman-Andino, J. W. Amoroso, D. P. DiPrete, H.-C. zur Loye, Flux crystal growth of the extended structure Pu(V) borate Na<sub>2</sub>(PuO<sub>2</sub>)(BO<sub>3</sub>). J. Am. Chem. Soc. 145, 10007–10014 (2023).
- H. B. Tisdale, M. S. Christian, G. Morrison, T. M. Besmann, K. Sun, G. Was, H.-C. zur Loye, Investigation of rare earth containing double phosphates of the type A<sub>3</sub>Ln(PO<sub>4</sub>)<sub>2</sub> (Ln = Y, La, Pr, Nd, Sm-Lu) as Potential Nuclear Waste Forms. Chem. Mater. 34, 3819–3830 (2022).
- A. T. Hines, G. Morrison, H. B. Tisdale, M. D. Smith, T. M. Besmann, A. Mofrad, K. Sun, G. Was, H.-C. zur Loye, Crystallization of A<sub>3</sub>Ln(BO<sub>3</sub>)<sub>2</sub> (A = Na, K; Ln = lanthanide) from a boric acid containing hydroxide melt: synthesis and investigation of lanthanide borates as potential nuclear waste forms. *Inorg. Chem.* 61, 11232–11242 (2022).
- S. J. Mugavero III, W. R. Gemmill, I. P. Roof, H.-C. zur Loye, Materials discovery by crystal growth: lanthanide metal containing oxides of platinum group metals (Ru, Os, Ir, Rh, Pd, Pt) from molten alkali metal hydroxides. J. Solid State Chem. 182, 1950–1963 (2009).
- 33. S. Wang, S.-J. Hwu,  $La_4Ti_5Si_{4-x}P_xO_{22}$  (x=0,1): A new family of two-dimensional solids. synthesis and structure of the first member (m=1) of the mixed-valence titanium(III/IV) oxosilicate series,  $La_4Ti(Si_2O_7)_2(TiO_2)_{4m}$ . Inorg. Chem. **34**, 166–171 (1995).
- J. L. Luce, A. M. Stacy, Crystallization of LnCu<sub>2</sub>O<sub>4</sub> (Ln = La, Nd, Sm, Eu, Gd, Dy, Ho, Y, Er) from hydroxide melts: Synthesis and structure. Chem. Mater. 9, 1508–1515 (1997).
- H. B. Tisdale, A. Mofrad, G. Morrison, T. M. Besmann, H.-C. zur Loye, Rb<sub>2</sub>Ln[Si<sub>2</sub>O<sub>6</sub>]F (Ln = Y, Eu-Lu): flux synthesis, structure determination, and DFT-calculated formation enthalpies of a series of mixed-anion rare earth cyclosilicates. *Inorg. Chem.* 62, 18440–18448 (2023).
- C. Juillerat, V. V. Klepov, G. Morrison, K. A. Pace, H.-C. zur Loye, Flux crystal growth: A versatile technique to reveal the crystal chemistry of complex uranium oxides. *Dalton Trans.* 48, 3162–3181 (2019).

- D. J. Cherniak, J. Pyle, J. Rakovan, Synthesis of REE and Y phosphates by Pb-free flux methods and their utilization as standards for electron microprobe analysis and in design of monazite chemical U-Th-Pb dating protocol. Am. Mineral. 89, 1533–1539 (2004).
- R. Podor, M. Cuney, Experimental study of Th-bearing LaPO<sub>4</sub> (780 C, 200 MPa): Implications for monazite and actinide orthophosphate stability. *Am. Mineral.* 82, 765–771 (1997).
- APEXIII Version 2016.5–0, SAINT Version 7.60A, SADABS Version 2016/2 (Bruker Analytical X-ray Systems, 2016).
- 40. G. M. Sheldrick, A short history of SHELX. Acta Crystallogr A. 64, 112-122 (2008).
- 41. G. M. Sheldrick, Integrated space-group and crystal-structure determination. *Acta Crystallogr. A* **71**, 3–8 (2015).
- O.V. Dolomanov, L. J. Bourhis, R. J. Gildea, H. A. K. Howard, H. Puschmann, OLEX2: a complete structure solution, refinement and analysis program. J. Appl. Cryst. 42, 339–341 (2009)
- A. L. Spek, Single-crystal structure validation with the program PLATON. J. Appl. Cryst. 36, 7–13 (2003).
- R. Dinnebier, A. Leineweber, J. Evans, Practical Powder Diffraction Pattern Analysis Using Topas (De Gruyter, 2019).

### Acknowledgments

Funding: Research was conducted by the Center for Hierarchical Waste Form Materials (CHWM), an Energy Frontier Research Center (EFRC). Research was supported by the US Department of Energy, Office of Basic Energy Sciences, Division of Materials Sciences and Engineering under award DE-SC0016574. This work was produced by Battelle Savannah River Alliance LLC under contract no. 89303321CEM000080 with the US Department of Energy. Publisher acknowledges the US Government license to provide public access under the DOE Public Access Plan (http://energy.gov/downloads/doe-public-access-plan). Author contributions: Writing—original draft: H.-C.z.L. and Y.Z. Conceptualization: H.-C.z.L., T.M.B., J.A., and Y.Z. Writing—review and editing: H.-C.z.L., T.M.B., J.A., Y.Z., H.B.T., N.K., G.M., M.D.S., and J.H. TEM: J.H. Methodology: H.-C.z.L., N.K., T.M.B., H.T., J.A., and Y.Z. Resources: H.-C.z.L., N.K., and T.M.B. Funding acquisition: H.-C.z.L. and J.A. Data curation: H.-C.z.L. Validation: H.-C.z.L., N.K., J.H., M.D.S., and Y.Z. Supervision: H.-C.z.L., G.M., and T.M.B. Formal analysis: H.-C.z.L., N.K., G.M., M.D.S., and Y.Z. Software: N.K. Project administration: H.-C.z.L., J.A., and Y.Z. Visualization: H.-C.z.L., N.K., J.H., H.B.T., and Y.Z. Investigation: J.H., H.B.T., and Y.Z. Synthesis: Y.Z. PXRD data collection and Rietveld analysis: H.B.T., N.K., and Y.Z. Single-crystal structure determination: G.M., M.D.S., and Y.Z. TEM: J.H. Chemical durability: J.A. Competing interests: The authors declare that they have no competing interests except that H.-C.z.L. is listed as an inventor on a provisional patent application #63/558,219 submitted by the University of South Carolina that covers the low-temperature synthesis process for making monazite. Data and materials availability: All data needed to evaluate the conclusions in the paper are present in the paper and/or the Supplemental Materials section. CCDC (deposition numbers: 2379894, 2379895, and 2379896) contains the supplementary crystallographic data for this paper. These data can be obtained free of charge via www.ccdc.cam.ac.uk/data\_request/cif, by emailing data\_ request@ccdc.cam.ac.uk, or by contacting The Cambridge Crystallographic Data Centre (12 Union Road, Cambridge CB2 1EZ, UK; fax: +44 1223 336033).

Submitted 24 September 2024 Accepted 14 February 2025 Published 21 March 2025 10.1126/sciady.adt3518